JOC The Journal of Organic Chemistry

Article

pubs.acs.org/joc

# Factors Controlling Selectivity in the Ring-Opening Metathesis Polymerization of 3-Substituted Cyclooctenes by Monoaryloxide Pyrrolide Imido Alkylidene (MAP) Catalysts

Henry Martinez,* Marc A. Hillmyer, and Christopher J. Cramer

Department of Chemistry, Chemical Theory Center, and Supercomputing Institute, University of Minnesota, 207 Pleasant Street SE, Minneapolis, Minnesota 55455, United States

Supporting Information

**ABSTRACT:** The origins of regio- and stereoselectivity in the ring-opening metathesis polymerization of 3-substituted *cis*-cyclooctenes by monoaryloxide pyrrolide imido alkylidene (MAP) Mo- and W-based catalysts are determined at the M06-2X/SDD|6-311+G(2df,p)//M06-L/SDD|6-31G(d)|MIDI! level of density functional theory. Considering *cis*-cyclooctene (COE) and 3-methyl-*cis*-cyclooctene (3MCOE) as monomers and W(N-*t*-Bu)(CH-*t*-Bu)(OHMT)(Pyr) (OHMT = hexamethylterphenoxide, Pyr = pyrrolide) as a catalyst, all possible *syn* and *anti* combinations of alkylidene and cyclic olefin, relative to the imido ligand, are evaluated. The observed *Z*-selectivity for the ring-opening metathesis (ROM) of COE is due to the large size of the aryloxide ligand, which forces both the alkylidene and the incoming cyclic olefin to be *syn* relative to the imido ligand. As determined previously for Grubbs' second-generation catalyst (G2), breakdown of the metallacyclobutane intermediate is the rate-limiting step for cyclic olefins having ring sizes exceeding five carbon atoms. Contrary to the G2 case, however, the ring-opening of 3MCOE by MAP catalysts prefers a *proximal* (3-substituent closest to the metal center) over a *distal* (3-substituent furthest from the metal center) approach. In all calculated paths, we observe inversion of catalyst configuration after each catalytic cycle.

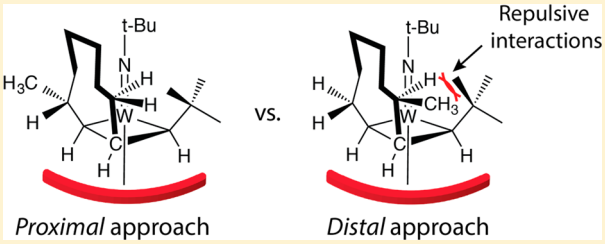


## INTRODUCTION

Ring-opening metathesis polymerization (ROMP) of both substituted and unsubstituted cyclic olefins leads to polymers with tunable physical properties.[1−3] The relative ease with which functionalized monomers may be synthesized, together with the development of highly active and functional group tolerant catalysts, makes ROMP an attractive method for the preparation of functionalized polymers. The asymmetric nature of most functionalized monomers, however, can lead to the synthesis of regio-irregular polymers with head-to-head (HH), head-to-tail (HT), and tail-to-tail (TT) microstructures and mixtures of *cis* and *trans* stereochemistry.[3] However, more precise control over microstructure can have significant impact on the final material properties, including higher melting temperature, increased tensile strength, and increased modulus in some cases.[3−6]

A number of Ru-, Mo-, and W-based compounds have proven to be effective ROMP catalysts. Of these three, Mo- and W-based catalysts demonstrate good control over stereo- and regioregularity, particularly in the ROMP of norbornene and norbornene derivatives.[7−11] The first generation of metal imido alkylidene bisalkoxide catalysts developed between 1986 and 1996 (Figure 1a) yielded *trans* syndiotactic polymers upon ROMP through a chain-end control mechanism.[9] Subsequently, metal alkylidene diolate catalysts were developed between 1996 and 2006 (Figure 1b).[9] The enantiomorphic site at the catalyst (e.g., with bisphenolate or binaphtholate ligands) yielded *cis* isotactic polymers. Since 2006, a new generation of Mo- and W-based catalysts have been designed (Figure 1c);[9,12] these metal imido alkylidene monoalkoxy pyrrolide (MAP) catalysts are the first to have a stereogenic metal center, yield *cis* syndiotatic polymers upon ROMP, and are the focus of the present work. Both experiments and calculations demonstrate that these asymmetric catalysts are more metathesis-active than those of prior generations,[13,14] which has been attributed to the difference in $\sigma$-donor strength between the two ligands (aryloxide vs pyrrolide): this causes the olefin to selectively approach the metal center *trans* to the better $\sigma$-donor pyrrolide

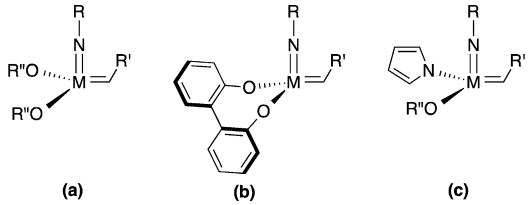


**Figure 1.** Different catalyst generations (M = W or Mo) used in the synthesis of polymers with controlled microstructure via ROMP. R, R′, and R″ are, in most examples, alkyl or aryl groups.

**Special Issue:** Mechanisms in Metal-Based Organic Chemistry

**Received:** July 29, 2014
**Published:** August 26, 2014

ligand.[9,14] While there is still a lack of understanding on the electronic reasons of why the olefin prefers to approach *trans* to the pyrrolide instead of the alkoxide ligand, computational calculations by Solans-Montfort et al. showed that lower energy is required to transform the catalyst from its tetrahedral form to the distorted trigonal bipyramid that accommodates the incoming olefin trans to the better $\sigma$-donor pyrrolide ligand.[14]

The *Z* selectivity of MAP W- and Mo-based catalysts is attributed mainly to the large size of the monoaryloxide ligand (R″), relative to the small imido ligand (R), which forces both the alkylidene and the approaching cyclic olefin to be *syn* relative to the imido ligand.[7,9] Figure 2 shows the polymerization of *cis*-cyclooctene (COE) by a (MAP)Mo-based catalyst and the generally accepted catalytic ROMP cycle. In this example, reported by Flook et al.,[7,8] poly(COE) was obtained in 99% *Z* configuration upon addition of Mo(NAd)(CHCMe$_2$Ph)(HIPTO)(Pyr) (Ad = 1-adamantyl, HIPTO = hexa(isopropyl)terphenoxide, Pyr = pyrrolide). In the catalytic cycle, the cyclooctene approaches the metal center *syn* to the imido ligand to form the Dewar−Chatt−Duncanson adduct (**Add**), followed by a [2+2] cycloaddition (**TS1**), which yields the metallacyclobutane (**MCB**) intermediate. This intermediate undergoes retro[2+2] cycloaddition (**TS2**) to yield the ring-opened product (**Prod**). Studies of W- and Mo-based catalysts have demonstrated that the **MCB** intermediate can adopt a square-pyramidal (SP) or trigonal-bipyramidal (TBP) conformation.[13−16] The geometry of the metallacyclobutane itself is planar in the TBP conformer, while in the SP conformer it is folded with the $\beta$-carbon pointing toward the imido group.[9,13−15] Computational studies have shown that upon [2+2] cycloaddition (through **TS1**) with ethylene, the TBP **MCB** intermediate is formed directly; however, the SP intermediate has been found to be the more stable isomer (0.6−7.0 kcal mol$^{-1}$) on the corresponding potential energy surface.[13,14] Considering the shape of these two conformers, the TBP **MCB** intermediate is closer in structure to the olefin/alkylidene complexes than the SP conformer.[13,14,17] Traditionally, TBP and SP conformers can be distinguished in terms of a geometrical parameter $\tau$ defined as $\tau = (\beta - \alpha)/60$, where $\beta$ is the largest angle from the ligand in the apical position to any other ligand and $\alpha$ is the largest angle between any two adjacent ligands in the basal plane. Thus, $\tau = 0$ for perfect SP structures and $\tau = 1$ for perfect TBP structures. However, a recent **MCB** intermediate has been described for which the $\tau$ value is close to that for a SP, but the geometry of the **MCB** is closer to that of a TBP by inspection.[18]

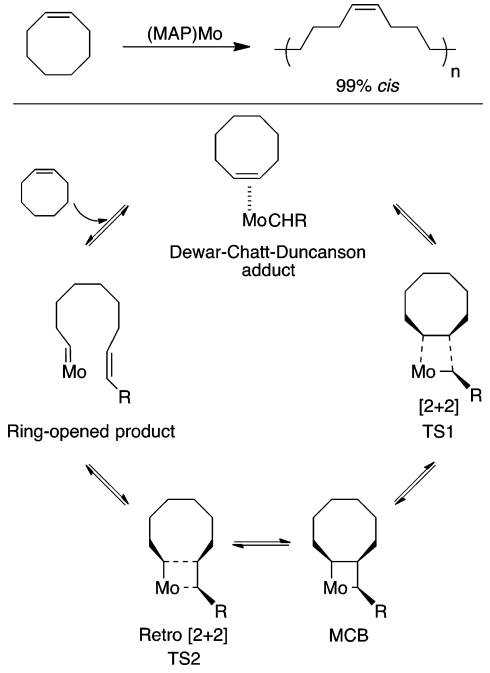


**Figure 2.** Synthesis of poly(*cis*-cyclooctene) by a Mo-based catalyst and the general mechanism of ring-opening metathesis polymerization (ROMP). Catalyst ligands removed for clarity.[7]

As mentioned previously, MAP W- and Mo-based catalysts provide not only *Z* stereoselectivity but also syndiotactic polymers.[7−9] While *Z* selectivity is attributed mainly to the large size of the monoaryloxide ligand, syndiotatic control is assigned to the ability of the catalyst to invert configuration after each catalytic cycle.[7−9] This causes the monomer to approach the metal center at a new CNO face that will always be *trans* to the pyrrolide ligand. Examples of this type of control have been observed during the polymerization of dicarbomethoxynorbornadiene and similar monomers.[7−9]

While the polymer microstructure has been controlled through the development of new catalysts, it has also been demonstrated that modifying the monomer unit can affect regioregularity. Recently, we reported that ROMP of a series of 3-substituted *cis*-cyclooctenes (3RCOE) yielded polymers with high stereo- (*trans*) and regioselectivity (HT) in the presence of Grubbs' second-generation catalyst (G2).[4,19,20] It was experimentally found that the degree of regioregularity increases with the size of the COE substituent. From this series of monomers, 3-alkyl-substituted *cis*-cyclooctenes have been polymerized by both G2 (>93% *trans*-HT) and, more recently, M(N-*t*-Bu)(CH-*t*-Bu)(OHMT)(Pyr) (OHMT = hexamethylterphenoxide, Pyr = pyrrolide, M = W or Mo) (>98% *cis*-HT) catalyst.[19,21] Both types of catalysts yield high HT polymers, but G2 gives primarily *E* configuration, while MAP catalysts give *Z* configuration (Figure 3). Interestingly,

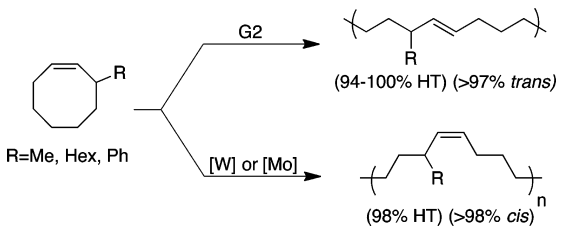


**Figure 3.** Synthesis of regio- and stereoselective poly(3-substituted *cis*-cyclooctenes) via ROMP.[19,21]

NMR experiments show that the propagating species of these two types of catalyst are different.[19,21] While the monomer approaches G2 in a *distal* manner (3-substituent farthest from metal center), for the MAP W and Mo-based catalysts, the *proximal* approach is favored (3-substituent closest to the metal center).

Computational studies using 3-methyl-*cis*-cyclooctene (3MCOE) as a substrate suggest that most of the observed regioselectivity obtained with G2 is due to steric interactions, with a minor enhancement from solvation effects.[22] The *proximal* approach, compared to the *distal* approach, is kinetically disfavored due to repulsive interactions between the substituent and the N-heterocyclic carbene (NHC) ligand. Understanding catalytic cycles at the microscopic level of detail


dx.doi.org/10.1021/jo501732q | J. Org. Chem. 2014, 79, 11940−11948

can lead to the design of next-generation catalysts with greater efficiency, as well as possibly greater regio-, and/or stereoselectivity. Motivated by this goal, we here investigate the origin of stereo- and regioselectivity in the ROMP of 3RCOE using MAP W- or Mo-based catalysts. 3MCOE and W(N-*t*-Bu)(CH-*t*-Bu)(OHMT)(Pyr) are taken as substrate monomer and catalyst, respectively.

## COMPUTATIONAL METHODS

**Density Functional Theory.** All stationary points were fully optimized at the M06-L level of density functional theory[23] employing the 6-31G(d) basis set[24] on the cyclooctene atoms as well as the alkylidene carbon and the MIDI! basis set[25] on all other nonmetal atoms. This combination of basis set for the nonmetal atoms was used in order to minimize the computing time without compromising the accuracy of the computed geometry. In addition, the (8s7p6d2f)/[6s5p3d2f] basis set and associated core potential of Andrae et al. was employed for W.[26] An automatically generated density-fitting basis set was employed to speed the computation of Coulomb integrals. Analytic frequency calculations were done for all structures in order to characterize their nature as either minima or TS structures, and also to compute thermal contributions to enthalpy and free energy employing the usual ideal-gas, rigid-rotator, and quasi-harmonic-oscillator approximation to compute necessary molar partition functions.[27,28]

For improved energetics of optimized structures, electronic energies were also computed using the M06-2X density functional,[29] which has been extensively benchmarked and shown to achieve high accuracies for organic systems; the basis set on nonmetal atoms for these single-point calculations was 6-311+G(2df,p).[24] Composite gas-phase free energies were then computed as the sum of M06-2X single-point electronic energies with M06-L thermal contributions computed as described above.

**Solvation.** M06-2X calculations identical to those described above were also performed including the effects of chloroform solvation as computed from the SMD continuum solvation model.[30] Composite free energies in solution were computed by summing gas-phase M06-L thermal contributions with single-point SMD/M06-2X single-point energies. Since the Gibbs free energies in the gas phase are calculated at 0.0446 M (1 atm) and in chloroform are reported for a standard state of 1 M, a standard-state concentration correction was made by adding 1.9 kcal mol$^{-1}$ ($RT$ ln ([soln]/[gas])) to the free energy for each molecule.

**Software.** All density functional calculations were accomplished with the Gaussian 09 suite of electronic structure programs revision A.02.[31]

## RESULTS

In our previous work, we found that COE has four conformers that might be expected to participate in ROMP at room temperature.[22] These four conformers correspond to two pairs of enantiomers with a 1.9 kcal mol$^{-1}$ free energy difference; only the lower energy pair is shown in Figure 4. We also found that with the G2 catalyst the reaction paths involving the higher energy enantiomeric pair failed to contribute significantly to olefin metathesis products,[22] so in this work we consider only the lower energy pair of enantiomers to compute the initiation step. Stationary points along this path include Dewar−Chatt−Duncanson complexes, [2+2] TS structures, **MCB** intermediates, and retro-[2+2] TS structures. Similarly, prior work found that of the four distinct allylic positions (**A**−**D**, Figure 4), conformers substituted at positions **B** and **C** were >4.5 kcal mol$^{-1}$ higher in free energy and also failed to contribute to olefin metathesis products compared to those substituted at either the **A** or **D** positions.[22] Consequently, only methyl group substitution in positions **A** and **D** was considered.

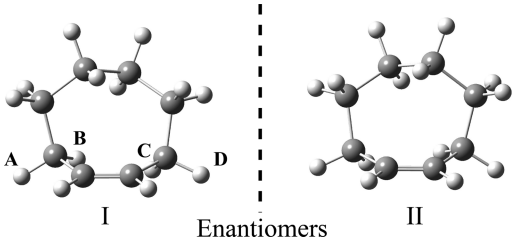


**Figure 4.** Low energy conformers of COE (I and II are an enantiomeric pair). Distinct allylic positions are labeled A, B, C, and D.[22]

Prior investigations have indicated that, for W- and Mo-based catalysts, the olefin can approach the metal center from either the side or the bottom approach relative to the imido ligand.[9,13,14] However, considerably less favorable energetics are associated with the bottom approach compared to the side alternative. The stereogenic nature of the metal center of the MAP catalysts (Figure 1c) leads to the availability of *two* side approaches, one that is *trans* to the pyrrolide ligand and the other that is *trans* to the aryloxide ligand. The better $\sigma$-donor ability of the pyrrolide ligand should cause the olefin to approach the side *trans* to this ligand (CNO face) in the absence of other influences.[14,32,33] Therefore, we restrict our consideration here to the pyrrolide *trans* approach. Although it has been reported that the *syn*-alkylidene, relative to the imido group, is more stable than the *anti*-alkylidene, both of these geometries are fully examined here.[9] Thus, considering one CNO face, the *syn*/*anti* geometry of the alkylidene and the *syn*/*anti* orientation of the incoming cyclic olefin, there are four distinct reaction paths depicted in Figure 5. There are eight distinct pathways when substitution at the **A** and **D** allylic positions is also considered.

We establish the following nomenclature for the stationary points along the ROM pathway: The Dewar−Chatt−Duncanson adduct (**Add**), [2+2] transition-state structure (**TS1**), metallacyclobutane intermediate (**MCB**), retro-[2+2] transition-state structure (**TS2**), and product (**Prod**). The lowest energy pair of enantiomers of *cis*-cyclooctene (COE) used in this work are named **I** and **II**, as above. Following our previous convention, the *proximal* approach (3-substituent closest to metal center) is defined by the methyl group at position **A**, while the *distal* approach (3-substituent farthest from the metal center) is defined by the methyl group at position **D**. Finally, the paths that yield *Z* and *E* products are named based on the orientation of the alkylidine (*syn* or *anti*) and COE (*syn* or *anti*) relative to the imido ligand. From Figure 5, "*syn*/*syn*" and "*anti*/*anti*" approaches lead to *Z* products, while "*syn*/*anti*" and "*anti*/*syn*" lead to *E* products. As an example, **IIA-*syn-anti*** corresponds to the energy pathway for COE enantiomer **II** with a methyl group in position **A** (*proximal* approach), the alkylidine *syn*, and the COE *anti*, both relative to the imido ligand, and yields an ***E*** double bond in the final product. All free energy values in this work are for 298 K and are reported relative to those of the isolated catalyst (W(N-*t*-Bu)(CH-*t*-Bu)(OHMT)(Pyr)) and most stable COE(**I**) or 3MCOE (**IA**) conformer, as appropriate.

The relevant stationary points on the potential energy surface corresponding to the four distinct reaction paths for the initiation step associated with the ROM of COE (Figure 5) have been calculated. Stationary points for the lowest energy path (**II-*syn-syn***) are shown in Figure 6, and the free energies (298 K) in chloroform for stationary points on *all* reactions


dx.doi.org/10.1021/jo501732q | J. Org. Chem. 2014, 79, 11940−11948

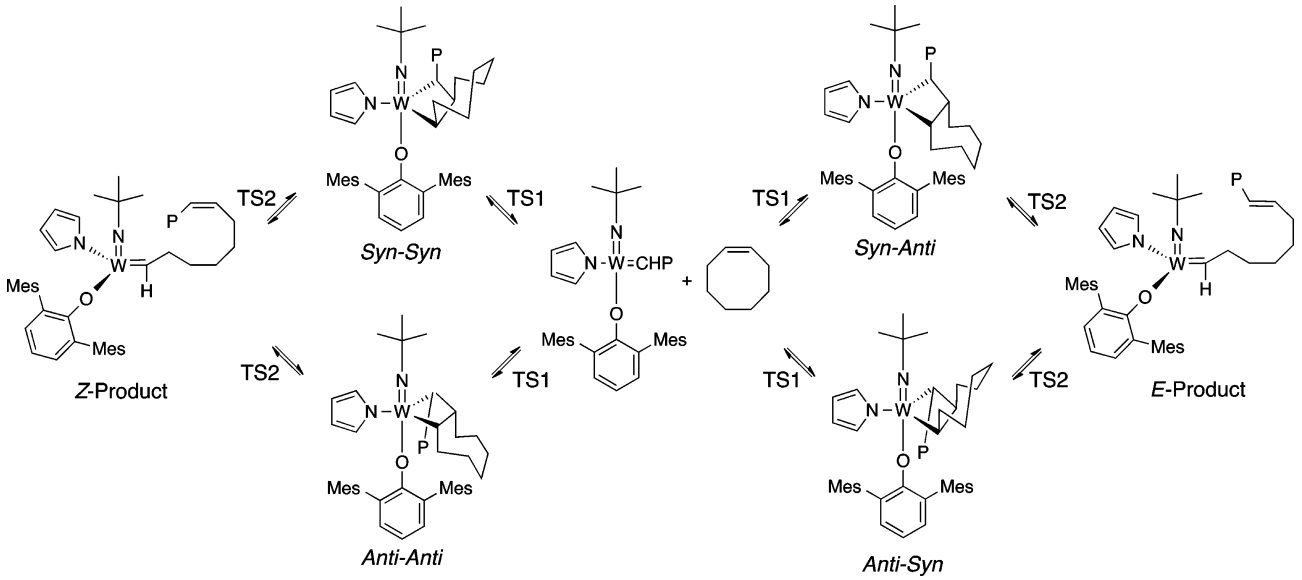


**Figure 5.** Possible pathways for the ROMP of COE by (MAP)W. Mes = mesityl, P = *tert*-butyl or polymer.

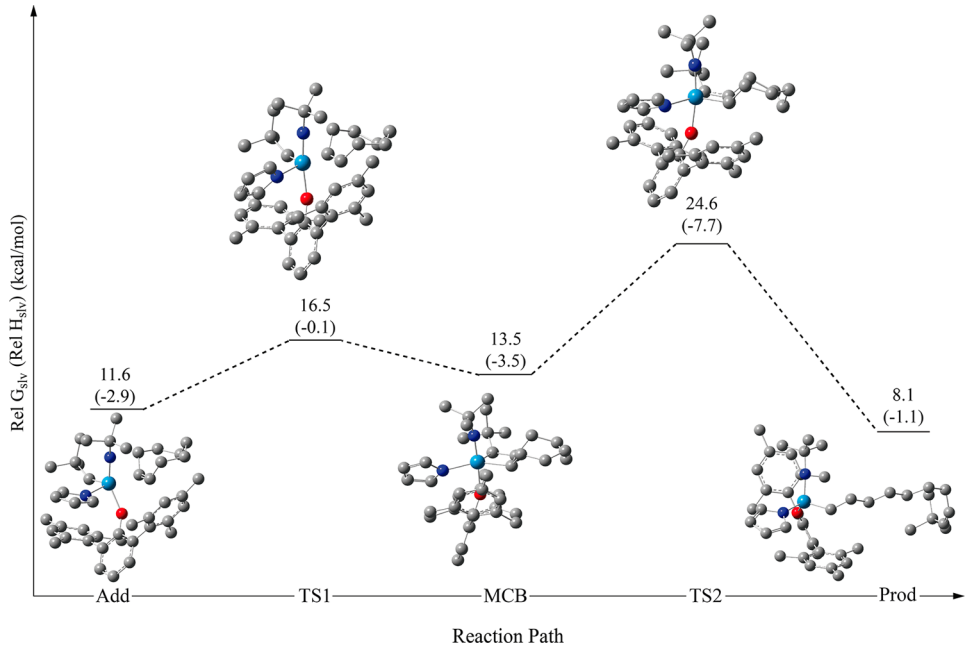


**Figure 6.** 298 K free energies in $CHCl_3$ (kcal $mol^{-1}$, enthalpies are in parentheses) for stationary points along the reaction path for **II-*syn-syn***. Carbon atoms are gray, nitrogen atoms are blue, oxygen atoms are red, tungsten is cyan, and hydrogen atoms are omitted for clarity.

paths are provided in Table 1. From Figure 6 and Table 1, one can see that in every instance the rate-limiting step (RLS) is the retro-[2+2] of the **MCB** intermediate. Although this is consistent with previous reports on the ROM of COE with G2,[22] it is contrary to other reports combining Mo- and W-based catalysts with smaller, cyclic olefins.[32,33] The product, calculated for the lowest energy path (**II-*syn-syn***), is 1.1 kcal/mol lower in enthalpy than separated reactants and 8.1 kcal/mol higher in free energy. Of course, this reaction occurs spontaneously at room temperature—the predicted endergonicity is associated with (i) using only a single-chain conformation in the product (which underestimates its entropy substantially),[22] (ii) leaving an open site on the metal, and (iii) a possible smaller driving force for initiation than for propagation. In any case, our focus here is on the factors

**Table 1. Relative 298 K Free Energies (kcal $mol^{-1}$) in $CHCl_3$ for Stationary Points on the *Z*- and *E*-Initiation Reaction Pathways for Both COE Enantiomers**

| | Add | TS1 | MCB | TS2 |
|---|---|---|---|---|
| I-*syn-syn* | 12.1 | 17.1 | 13.7 | 25.9 |
| I-*anti-anti* | 22.4 | 29.7 | 27.5 | 36.8 |
| I-*anti-syn* | 18.0 | 19.7 | 17.3 | 30.0 |
| I-*syn-anti* | 14.5 | 18.3 | 13.3 | 27.5 |
| **II-*syn-syn*** | **11.6** | **16.5** | **13.5** | **24.6** |
| II-*anti-anti* | 23.6 | 30.1 | 28.4 | 36.1 |
| II-*anti-syn* | 17.6 | 20.4 | 16.0 | 28.2 |
| II-*syn-anti* | 14.9 | 18.4 | 12.6 | 26.4 |


dx.doi.org/10.1021/jo501732q | *J. Org. Chem.* 2014, 79, 11940−11948

affecting the energetics of rate-determining transition-state structures, and we will now consider these in more detail.

The calculated free energies of activation for the RLSs (**TS2** in every case, Table 1) were used to predict a Boltzmann-weighted product distribution (Table 2). The *Z* product is predicted to have a population of 95%, deriving only from the **II-*syn-syn*** pathway. The 5% of predicted *E* product comes from approach of COE *anti* to a *syn*-alkylidene, mostly as conformer **II** but with some contribution from **I**. These values are in good agreement with the experimental results of Flook et al., where poly(COE) was obtained in a 99% *Z*-configuration.[7] It is of interest to note that the predicted *Z*:*E* ratio for this reaction in the gas phase is only 76:24; i.e., solvation contributes significantly to the increased stereoselectivity.

**Table 2. 298 K Boltzmann-Weighted Product Populations for COE Initiation in $CHCl_3$**

| | $G_{rel}$ **TS2** (kcal mol$^{-1}$) | population | total (%) |
|---|---|---|---|
| **I-*syn-syn*** | 1.3 | 0.10 | 95 |
| **I-*anti-anti*** | 12.2 | 0.00 | |
| **II-*syn-syn*** | 0.0 | 0.85 | |
| **II-*anti-anti*** | 11.5 | 0.00 | |
| **I-*anti-syn*** | 5.4 | 0.00 | 5 |
| **I-*syn-anti*** | 2.9 | 0.01 | |
| **II-*anti-syn*** | 3.6 | 0.00 | |
| **II-*syn-anti*** | 1.8 | 0.04 | |

The results for the four initiation paths for the ROM of COE were taken as a starting point for corresponding paths with 3MCOE. Considering that the *anti-anti* and *anti-syn* paths were significantly higher in free energy for COE (Table 1), we only calculated the *syn-syn* and *syn-anti* paths for the ROM of 3MCOE. 3MCOE can approach the metal center in either the *proximal* approach (3-substituent closest to the metal center) or *distal* approach (3-substituent farthest from metal center) (Figure 7), and it is the selectivity for one approach over the other that leads to the observed regioselectivity. We considered both approaches in this work. Although G2 and MAP W- and Mo-based catalysts give high regioselectivity, NMR experiments have demonstrated that the propagating species of these two catalysts types are different (*distal* approach for G2 and *proximal* approach for the MAP catalysts).[19,21]

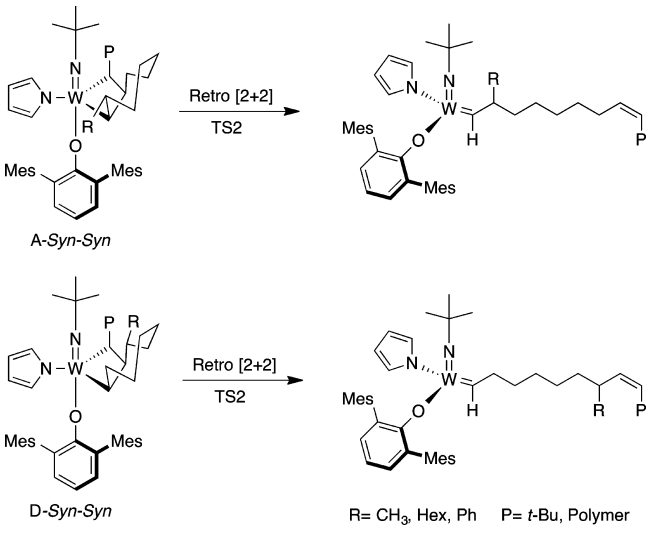


**Figure 7.** Possible propagating metallacyclobutane intermediates that lead to the formation of *cis*, HT regioisomer in the ROMP of 3RCOE by (MAP)W catalysts: *proximal* approach (top) and *distal* approach (bottom).

Table 3 shows the 298 K free energies in chloroform for stationary points along the *proximal* and *distal* reaction paths for both the *syn-syn* and *syn-anti* orientations. Consistent with the results for the unsubstituted COE, the breakdown of the **MCB** intermediate (**TS2**) is still the RLS for 3MCOE. From Table 3, it is clear that all four *proximal* paths (**A**) are considerably lower in free energy than the *distal* paths (**D**). This is consistent with the NMR results in which the methyl substituent is close to the metal center after the ring opening of 3MCOE in the presence of excess MAP catalyst.[21] The lowest free energy path, **IIA-*syn-syn*** (bold in Table 3), indicates that the *Z*-product is also preferred. Table 4 provides the Boltzmann-weighted product distributions derived from the RLS free energies of activation in Table 3. The *distal*/*syn-syn* path is predicted to account for 100% of product at 298 K in chloroform. This preference is consistent with the experimental results. In the gas phase, this path is 99% preferred, i.e., solvation ($CHCl_3$) still plays some role, but to a lesser extent than for COE. The remaining 1% in the gas phase comes from the *distal*/*syn-anti* path (**IIA-*syn-anti***, see the Supporting Information).

**Table 3. Relative 298 K Free Energies (kcal mol$^{-1}$) in $CHCl_3$ for Stationary Points on Initiation Reaction Pathways for Selected 3MCOE Conformers**

| | **Add** | **TS1** | **MCB** | **TS2** |
|---|---|---|---|---|
| **IA-*syn-syn*** | 15.6 | 23.2 | 20.5 | 26.8 |
| **IA-*syn-anti*** | 14.9 | 18.2 | 14.3 | 29.4 |
| **IIA-*syn-syn*** | **13.6** | **22.2** | **20.6** | **24.2** |
| **IIA-*syn-anti*** | 15.0 | 18.0 | 13.1 | 28.2 |
| **ID-*syn-syn*** | 17.0 | 31.4 | 29.9 | 35.3 |
| **ID-*syn-anti*** | 15.9 | 24.5 | 20.6 | 33.0 |
| **IID-*syn-syn*** | 16.0 | 30.6 | 27.8 | 36.4 |
| **IID-*syn-anti*** | 16.3 | 25.7 | 20.0 | 30.8 |

**Table 4. 298 K Boltzmann-Weighted Product Populations for 3MCOE Initiation in $CHCl_3$**

| | $G_{rel}$ **TS2** (kcal mol$^{-1}$) | population | total (%) |
|---|---|---|---|
| **IA-*syn-syn*** | 2.6 | 0.01 | 100 |
| **IA-*syn-anti*** | 5.2 | 0.00 | |
| **IIA-*syn-syn*** | 0.0 | 0.99 | |
| **IIA-*syn-anti*** | 4.0 | 0.00 | |
| **ID-*syn-syn*** | 11.1 | 0.00 | 0 |
| **ID-*syn-anti*** | 8.8 | 0.00 | |
| **IID-*syn-syn*** | 12.2 | 0.00 | |
| **IID-*syn-anti*** | 6.6 | 0.00 | |

## DISCUSSION

**ROM of COE.** Coordination of the cyclic olefin to the metal center on the CNO face to form the Dewar−Chatt−Duncanson adduct takes the catalyst from its tetrahedral geometry to a pseudotrigonal bipyramid. The pyrrolide ligand takes an equatorial position, *trans* relative to the incoming


dx.doi.org/10.1021/jo501732q | J. Org. Chem. 2014, 79, 11940−11948

olefin, while the aryloxide takes an axial position, as might be expected given its size compared to the other ligands. The [2+2] cycloaddition (**TS1**), which proceeds in a concerted and asynchronous fashion, leads to the formation of a **MCB** intermediate with a TBP geometry. The concerted, asynchronous breakdown of the **MCB** (**TS2**) leads to the formation of a new double bond and completes one step of the catalytic cycle. **TS2** is the RLS in all cases, but with higher free energy for those paths in which the cyclic olefin reacts with the *anti*-alkylidene, or those in which the cyclic olefin approaches the metal in the *anti*-orientation, relative to the imido ligand. This is consistent with the large aryloxide ligand forcing all other atoms away to avoid repulsive steric interactions, and leads to the *Z*-product. The pyrrolide ligand, which started *trans* to the double bond of the incoming cyclic olefin, moves along the equatorial plane to assume a *trans* orientation relative to the newly formed double bond. This pyrrolide ligand shift manifests the inversion of configuration at the metal center after each catalytic cycle.

Previous gas-phase computational calculations in the ROM of cyclopropene[32,33] showed that the RLS is the [2+2] cycloaddition, which contrasts with our results for the ROM of COE, where the breakdown of the **MCB** (**TS2**) is the RLS. To validate our results, the potential energy surface for the ROMs of cyclopentene and cycloheptene were calculated in the gas phase at the composite M06-2X level and compared to those with COE (Table 5). Similar to previous findings with

**Table 5. Relative Gas-Phase 298 K Free Energies (kcal mol$^{-1}$) for Stationary Points Associated with the ROMP of *Z*-Cyclopentene 5, *Z*-Cycloheptene 7, and *Z*-Cyclooctene 8**

| ring size | Add | TS1 | MCB | TS2 |
|---|---|---|---|---|
| 5 | 12.5 | 16.8 | 5.9 | *a* |
| 7 | 12.8 | 15.5 | 11.2 | 22.1 |
| 8 | 9.3 | 15.9 | 13.3 | 24.0 |

[a]Stationary point not found.

G2,[22] the free energy of **TS1** for all three rings is similar (Table 5). The stability of the **MCB** decreases as the ring size increases, and **TS2** becomes the RLS with rings larger than 5. We made several unsuccessful attempts to find **TS2** for the ROM of cyclopentene. Although we found a minimum for the **MCB** intermediate, all distortions along any path designed to find **TS2** simply led to the formation of product, presumably owing to a very flat potential energy surface along the reaction coordinate and some numerical noise associated with non-analytic density functional integrals determined on necessarily finite integration grids; such situations can defeat optimization algorithms in their search for a stationary TS structure. We conclude that the free energy of the retro-[2+2] transition-state structure must be only very slightly higher than that of the **MCB** intermediate. It is thus evident that the change in RLS from **TS1** to **TS2** is driven mainly by the increase in repulsive interactions between the larger rings and the alkylidene that become more severe in the more expanded retro-[2+2] cycloaddition transition-state structure than in the more compact **MCB** intermediate

The *Z* selectivity observed for MAP catalysts is primarily attributable to the large size of the aryloxide ligand. Table 1 shows that, with the exception of the *anti-anti* paths, the relative free energies for all **MCB** intermediates are roughly the same. Therefore, there must be considerations specific to **TS2** that dictate the predicted variation in activation free energies. Table 6 shows selected valence bond angles for both the **MCB** and

**Table 6. Selected M06-L Valence Bond Angles (deg) for MCB and TS2 Structures on COE Initiation Pathways**

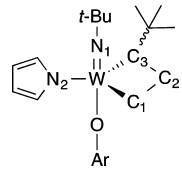


| | MCB | TS2 |
|---|---|---|
| | N1−W−O | N1−W−O |
| I-*syn-syn* | 169 | 171 |
| I-*anti-anti* | 154 | 157 |
| I-*anti-syn* | 162 | 152 |
| I-*syn-anti* | 168 | 156 |
| II-*syn-syn* | 170 | 171 |
| II-*anti-anti* | 156 | 157 |
| II-*anti-syn* | 161 | 154 |
| II-*syn-anti* | 168 | 157 |

**TS2** structures during the ROM of COE. With the exception of the *anti-anti* **MCB** intermediates, the N1−W−O angle is closer to the 180° expected for a TBP conformer. The higher free energy observed for the *anti-anti* **MCB** intermediates (Table 1) derives from the repulsive interactions between the *anti*-alkylidene and the *anti*-cyclic olefin with the aryloxide ligand. This interaction bends the N1−W−O angle and distorts the TBP structure. During the breakdown of the **MCB** intermediate, through **TS2**, a more significant geometric difference is observed between the different paths which affects the energetics of the RLSs (Table 1). While the *syn-syn* paths preserve N1−W−O angles close to 180°, all other paths with an *anti* alkylidene or *anti* olefin give rise to a distorted TBP structure (N1−W−O angle <160°) and a corresponding increase in the activation free energy.

We now return to the observation that solvent increases the *Z*/*E* preference from 76:24 to 95:5. Table 7 shows the M06-2X

**Table 7. M06-2X Dipole Moments (D) for TS Structures on the *Z* and *E* Initiation Reaction Pathways for Both COE Enantiomers**

| | TS1 | TS2 |
|---|---|---|
| I-*syn-syn* | 5.49 | 5.69 |
| I-*anti-anti* | 4.96 | 4.97 |
| I-*anti-syn* | 5.88 | 5.56 |
| I-*syn-anti* | 5.14 | 4.47 |
| II-*syn-syn* | 5.48 | 5.55 |
| II-*anti-anti* | 5.02 | 4.94 |
| II-*anti-syn* | 5.69 | 5.41 |
| II-*syn-anti* | 5.30 | 4.53 |

dipole moments (D) for the various TS structures on the *Z* and *E* initiation reaction pathways of COE. From Table 7, one can see that the small solvent effect that favors *Z* selectivity derives from the larger dipole moments of the *syn-syn* paths at the RLS. Although the *anti-syn* paths also have large dipole moments, steric repulsive interactions dominate the stereoselectivity for those cases.


dx.doi.org/10.1021/jo501732q | *J. Org. Chem.* 2014, 79, 11940−11948

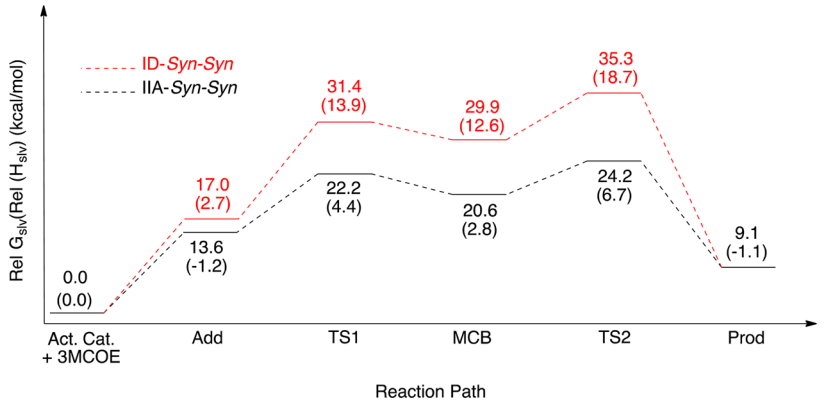


**Figure 8.** 298 K free energies in $CHCl_3$ (kcal $mol^{-1}$, enthalpies are in parentheses) for stationary points along the reaction paths for **IIA-*syn-syn*** and **ID-*syn-syn***, the lowest free energy *cis* reaction paths for the various **A** and **D** approaches.

**ROM of 3MCOE.** Based on our previous work,[22] only the four lowest energy diastereomeric pairings of 3MCOE enantiomers with catalyst were considered for the calculation of the potential energy surfaces in the ROM with W(N-*t*-Bu)(CH-*t*-Bu)(OHMT)(Pyr). Figure 8 shows the lowest free energy paths for both *proximal* (**IIA-*syn-syn***) and *distal* (**ID-*syn-syn***) approaches that lead to the formation of *Z*-product. The *proximal* approach is in every case lower in free energy than the *distal* approach, and breakdown of the **MCB** (through **TS2**) is the RLS for both approaches. The free energies in $CHCl_3$ for the ROM of 3MCOE (Table 3) show that, while the formation of the Dewar−Chatt−Duncanson adduct has similar free energies along all paths, the free energy difference increases between the *proximal* and *distal* approaches as the reaction proceeds further along the reaction paths. In all paths, the breakdown of the **MCB** (through **TS2**) is the RLS, and the Boltzmann-weighted product populations completely (100%) favor the *proximal* approach. While the *syn-syn* orientations dominate in both the gas phase and in solvent, the value of the *Z*-selectivity increases from 99 to 100% upon inclusion of the solvent. A similar solvent effect was observed for the unsubstituted COE, but to a larger extent. Thus, formation of the *Z*-product having the methyl group closest to the metal center is predicted to be a single product in $CHCl_3$. As found for the unsubstituted COE, the pyrrolide ligand moves in the equatorial plane along the reaction path leading to an inversion of configuration at the metal center after each catalytic cycle. Interestingly, when the two lowest free energy paths for COE and 3MCOE (**II-*syn-syn*** and **IIA-*syn-syn***, respectively) are compared, there is a significant free energy difference up to the breakdown of the **MCB** intermediate, where the free energies are almost identical. Considering that this is the RLS in both paths, one would expect these two reactions to proceed at very similar rates.

A close look at the **MCB** intermediates of the 3MCOE paths shows that in the *distal* approach there are significant repulsive interactions between the methyl substituent and the *tert*-butyl alkylidene (Figure 9). Such interactions, which are absent in the *proximal* approach, are also present at the RLS (**TS2**) and are responsible for the observed regioselectivity of the W(N-*t*-Bu)(CH-*t*-Bu)(OHMT)(Pyr) catalyst. In order to evaluate the impact of these repulsive interactions, we tabulated selected valence bond angles for both the **MCB** intermediates and TS 2s (Table 8). To analyze the data in Table 8, we take the unsubstituted COE structures as a reference and consider this structure to have the most favorable interactions between the allylic hydrogens and any other ligand. Table 8 shows that while the C5−C2−C3 and C2−C3−C4 angles remain almost invariant for the *proximal* approach, the angles increase for

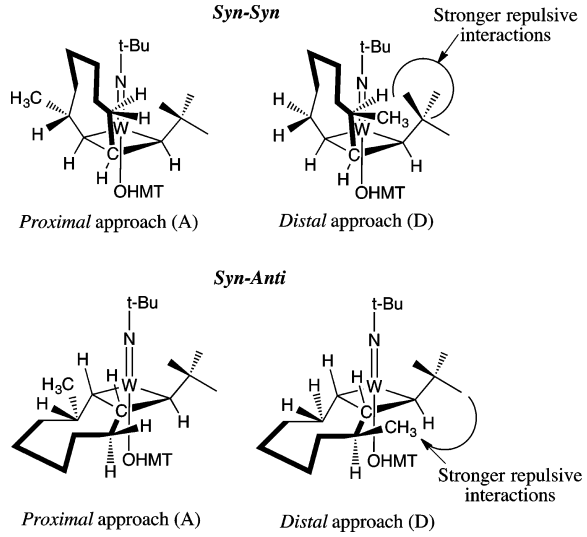


**Figure 9. MCB** intermediates that lead to the formation of different stereo- and regiospecific products. OHMT stands for hexamethylterphenoxide. The pyrrole ligand omitted for clarity.

**Table 8. Selected M06-L Valence Bond angles (deg) for MCB and TS2 Structures on COE and 3MCOE Initiation Pathways**

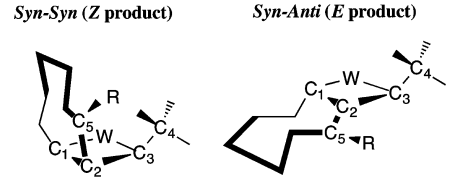


| | MCB | | TS2 | |
|---|---|---|---|---|
| | C5−C2−C3 | C2−C3−C4 | C5−C2−C3 | C2−C3−C4 |
| **II-*syn-syn*** | 114 | 126 | 124 | 129 |
| **II-*syn-anti*** | 111 | 118 | 120 | 121 |
| **IIA-*syn-syn*** | 112 | 127 | 123 | 127 |
| **IIA-*syn-anti*** | 112 | 117 | 121 | 121 |
| **IID-*syn-syn*** | 120 | 134 | 129 | 135 |
| **IID-*syn-anti*** | 116 | 119 | 122 | 120 |


dx.doi.org/10.1021/jo501732q | *J. Org. Chem.* 2014, 79, 11940−11948

the *distal* approach. These changes indicate stress in the structures and increase their free energies. We note that for the *distal syn-syn* path, both the C5−C2−C3 and C2−C3−C4 angles change significantly, while for the *distal syn-anti* path, it is the C2−C3−C4 angle that changes the most.

Subsequent to ROM of the first 3MCOE, following the lowest free energy path (**IIA-*syn-syn***), the new alkylidene has a methyl group closer to the metal center. This new alkylidene is substituted with the approximate equivalent of a *sec*-butyl group, which is still somewhat bulky. Since the results suggest that the interactions between the substituent and the *tert*-butyl alkylidene are the ones responsible for the regioselectivity, we assessed the influence of a less bulky alkylidene by replacing it with the less bulky, linear *n*-butyl alkylidene. We then calculated the breakdown of the **MCB** intermediate (**TS2**) along the *syn-syn* path for both the *distal* and *proximal* approaches with the *n*-butyl alkylidene (Table 9). The results shown in Table 9 indicate that the catalyst will still be highly regioselective even with the less bulky *n*-butyl alkylidene. While the overall free energies of activation associated with **TS2** are lower than those with the *tert*-butyl alkylidene, *proximal* is still preferred over *distal* by a significant margin.

**Table 9. Relative 298 K Free Energies (kcal mol$^{-1}$) in $CHCl_3$ for the Retro-[2+2]-cycloaddition (TS2) with a Linear Alkylidene Ligand (*n*-Butyl) for Selected 3MCOE Conformers on the *Z* initiation Reaction Pathway and Associated Boltzmann-Weighted Product Populations**

| | TS2 | $G_{rel}$ TS2 (kcal mol$^{-1}$) | population | total (%) |
|---|---|---|---|---|
| IA-*syn-syn-n*Bu | 14.8 | 0.3 | 0.36 | 100 |
| IIA-*syn-syn-n*Bu | 14.5 | 0.0 | 0.64 | |
| ID-*syn-syn-n*Bu | 21.6 | 7.1 | 0.00 | 0 |
| IID-*syn-syn-n*Bu | 19.7 | 5.2 | 0.00 | |

Considering conformational issues in the metathesis intermediates, previous reports have indicated that SP **MCB** intermediates are more stable than the corresponding TBP isomer.[13,14,17,32,33] However, only the TBP **MCB** intermediate undergoes retro[2+2] to generate the product. In our calculated structures, the [2+2] cycloaddition (**TS1**) leads to the formation of the **MCB** intermediate with a TBP geometry. We computed the geometric and free energy differences between the SP and TBP **MCB** intermediates of both COE and 3MCOE for those pathways that contribute to product formation, i.e., **I-*syn-syn*** and **II-*syn-syn*** for COE and **IIA-*syn-syn*** for 3MCOE (Table 10). While the TBP **MCB** intermediates calculated in this work have M−C($\alpha$) distances between 2.03 and 2.09 Å and M−C($\beta$) distances of about 2.41 Å, the minima found for the SP **MCB** intermediates exhibit distances that average 2.19 and 2.81 Å for the M−C($\alpha$) and M−C($\beta$) bond lengths, respectively. As expected, the TBP **MCB** intermediates have approximately planar cyclobutane rings and the SP **MCB** intermediates have a more folded ring structure with the $\beta$ carbon pointing toward the imido ligand. The results shown in Table 10 indicate that for the second lowest COE free energy path (**I-*syn-syn***), there is a small free energy difference in favor of the SP intermediate. However, for the lowest COE free energy path (**II-*syn-syn***) the TBP structure is actually more stable than SP. While this result was unexpected, Solans-Montfort et al.[14] made a similar observation when investigating the role of the pyrrolide ligand in a silica-supported catalyst for alkene metathesis. The lowest free energy path for 3MCOE shows a larger free energy difference (3.1 kcal mol$^{-1}$) between the two **MCB** conformers. Although the reason for the small swap in relative stabilities between the SP and TBP **MCB** intermediates for I and II COE is unclear, it is clear that the methyl group destabilizes the TBP **MCB** intermediate for those structures derived from IIA versus II. When comparing the structures, one can see that the methyl group in IIA is introduced in such a way that it clashes with a mesityl group on the aryloxide ligand and thus destabilizes the TBP **MCB** intermediate. This interaction is not present in the SP structure. The transition-state structures for the interconversion between the TBP and SP conformers for the **II-*syn-syn*** and **IIA-*syn-syn*** paths were calculated to have relative free energies of 22.5 and 25.7 kcal mol$^{-1}$, respectively ($CHCl_3$, relative to separated reactants). Along the **IIA-*syn-syn*** path, this interconversion has a higher activation free energy than that for continued reaction through **TS2** (the RLS). As this conformational equilibrium does not affect product distribution, however, there is no effect on the overall kinetics of the ROM of 3MCOE nor on predicted regio- and stereoselectivities.

**Table 10. Relative 298 K Free Energies (kcal mol$^{-1}$) in $CHCl_3$ of MCB Conformers for the Lowest Energy Initiation Reaction Pathways for COE and 3MCOE**

| | MCB-TBP | MCB-SP |
|---|---|---|
| I-*syn-syn* | 13.7 | 13.4 |
| II-*syn-syn* | 13.5 | 15.3 |
| IIA-*syn-syn* | 20.6 | 17.5 |

## CONCLUSIONS

In this work, we studied the ROM of both COE and 3MCOE with W(N-*t*-Bu)(CH-*t*-Bu)(OHMT)(Pyr) as a catalyst. Similar to what we previously found with the Grubbs' second-generation catalyst (G2),[22] the breakdown of the **MCB** intermediate is the RLS for cyclic olefins having ring sizes exceeding five carbon atoms. This is mainly driven by the increase in repulsive interactions between the ring and the alkylidene ligand. The high *Z* stereoselectivity observed in the ROM of COE comes mostly from the larger size of the aryloxide ligand, which forces both the alkylidene and the incoming cyclic olefin to be *syn* relative to the imido ligand. Solvation effects slightly favor the *Z* product paths due to greater polarity of the relevant transition-state structures.

The ROM of 3MCOE prefers *proximal* over *distal* approach, as significant repulsive interactions between the methyl substituent and either the *tert*-butyl alkylidene or growing polymer chain are present in the latter. We observed in all calculated paths inversion of configuration after each catalytic cycle. The ability of the pyrrolide ligand to move on the equatorial plane along the reaction path to remain *trans* to either the incoming or newly formed double bond is what causes the inversion of configuration at the metal center.

When comparing the **MCB** intermediates for the lowest reaction path of Grubbs' second-generation (G2) and W(N-*t*-Bu)(CH-*t*-Bu)(OHMT)(Pyr) catalysts (Figure 10), one can see that in both catalysts the large ligands play an important role in the regio- and stereoselectivity. While the approach of the cyclic olefin varies between these two catalysts (relative to the large ligand), the repulsive interaction between the large ligand and the allylic substituent is the driving force for the


dx.doi.org/10.1021/jo501732q | J. Org. Chem. 2014, 79, 11940−11948

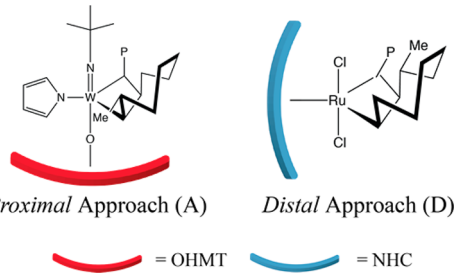


**Figure 10. MCB** intermediates for the lowest reaction path of each W(N-*t*-Bu)(CH-*t*-Bu)(OHMT)(Pyr) (left) and Grubbs' second-generation (right) catalysts.

regio- and stereoselection. The observations of this study help to more thoroughly define the mechanism of MAP catalysts. In addition, these results can serve as a guide for monomer and catalyst design allowing for the tunability of polymer properties.

## ■ ASSOCIATED CONTENT

### Supporting Information

Free energies and enthalpies (kcal/mol) in both the gas phase and chloroform solution for all calculated potential energy surfaces. Cartesian coordinates for all structures optimized at the M06-L/SDD|6-31G(d)|MIDI! level of theory are provided as well. This material is available free of charge via the Internet at http://pubs.acs.org.

## ■ AUTHOR INFORMATION

### Corresponding Author

*E-mail: hmartine@umn.edu.

### Notes

The authors declare no competing financial interest.

## ■ REFERENCES

(1) Bielawski, C. W.; Grubbs, R. H. *Prog. Polym. Sci.* **2007**, *32*, 1.
(2) Schrock, R. R. *Acc. Chem. Res.* **1990**, *23*, 158.
(3) Martinez, H.; Ren, N.; Matta, M.; Hillmyer, M. A. *Polym. Chem.* **2014**, *5*, 3507.
(4) Zhang, J.; Matta, M. E.; Martinez, H.; Hillmyer, M. A. *Macromolecules* **2013**, *46*, 2535.
(5) Rojas, G.; Berda, E. B.; Wagener, K. B. *Polymer* **2008**, *49*, 2985.
(6) Rojas, G.; Wagener, K. B. *Macromolecules* **2009**, *42*, 1934.
(7) Flook, M. M.; Jiang, A. J.; Schrock, R. R.; Muller, P.; Hoveyda, A. H. *J. Am. Chem. Soc.* **2009**, *131*, 7962.
(8) Flook, M. M.; Ng, V. W. L.; Schrock, R. R. *J. Am. Chem. Soc.* **2011**, *133*, 1784.
(9) Schrock, R. R. *Dalton Trans.* **2011**, *40*, 7484.
(10) Forrest, W. P.; Weis, J. G.; John, J. M.; Axtell, J. C.; Simpson, J. H.; Swager, T. M.; Schrock, R. R. *J. Am. Chem. Soc.* **2014**, *136*, 10910.
(11) Schrock, R. R. *Acc. Chem. Res.* **2014**, *47*, 2457.
(12) Singh, R.; Schrock, R. R.; Muller, P.; Hoveyda, A. H. *J. Am. Chem. Soc.* **2007**, *129*, 12654.
(13) Poater, A.; Solans-Montfort, X.; Clot, E.; Coperet, C.; Eisenstein, O. *J. Am. Chem. Soc.* **2007**, *129*, 8207.
(14) Solans-Montfort, X.; Coperet, C.; Eisenstein, O. *J. Am. Chem. Soc.* **2010**, *132*, 7750.
(15) Schrock, R. R.; Jiang, A. J.; Marinescu, S. C.; Simpson, J. H.; Muller, P. *Organometallics* **2010**, *29*, 5241.
(16) Feldman, J.; Davis, W. M.; Schrock, R. R. *Organometallics* **1989**, *8*, 2266.
(17) Goumans, T. P. M.; Ehlers, A. W.; Lammertsma, K. *Organometallics* **2005**, *24*, 3200.
(18) Reithofer, M. R.; Dobereiner, G. E.; Schrock, R. R.; Muller, P. *Organometallics* **2013**, *32*, 2489.
(19) Kobayashi, S.; Pitet, L. M.; Hillmyer, M. A. *J. Am. Chem. Soc.* **2011**, *133*, 5794.
(20) Martinez, H.; Zhang, J.; Kobayashi, S.; Xu, Y.; Pitet, L. M.; Matta, M.; Hillmyer, M. A. *Appl. Petrochem. Res.* **2014**, DOI: 10.1007/s13203-014-0048-z.
(21) Jeong, H.; Kozera, D. J.; Schrock, R. R.; Stacey J. Smith, S. J.; Zhang, J.; Ren, N.; Hillmyer, M. A. *Organometallics* **2013**, *32*, 4843.
(22) Martinez, Henry; Miro, Pere; Charbonneau, Patrick; Hillmyer, Marc A.; Cramer, Christopher J. *ACS Catal.* **2012**, *2*, 2547.
(23) Zhao, Y.; Truhlar, D. G. *J. Chem. Phys.* **2006**, *125*, 194101.
(24) Hehre, W. J.; Radom, L.; Schleyer, P. v. R.; Pople, J. A. *Ab Initio Molecular Orbital Theory*; Wiley: New York, 1986.
(25) Easton, R. E.; Giesen, D. J.; Welch, A.; Cramer, C. J.; Truhlar, D. G. *Theor. Chim. Acta.* **1996**, *93*, 281.
(26) Andrae, D.; Häußermann, U.; Dolg, M.; Stoll, H.; Preuß, H. *Theor. Chem. Acta* **1990**, *77*, 123.
(27) Cramer, C. J. *Essentials of Computational Chemistry: Theories and Models*; 2nd ed.; John Wiley & Sons: Chichester, 2004.
(28) Ribeiro, R. F.; Marenich, A. V.; Cramer, C. J.; Truhlar, D. G. *J. Phys. Chem. B* **2011**, *115*, 14556.
(29) Zhao, Y.; Truhlar, D. G. *Acc. Chem. Res.* **2008**, *41*, 157.
(30) Marenich, A. V.; Cramer, C. J.; Truhlar, D. G. *J. Phys. Chem. B* **2009**, *113*, 6378.
(31) Frisch, M. J.; Trucks, G. W.; Schlegel, H. B.; Scuseria, G. E.; Robb, M. A.; Cheeseman, J. R.; Scalmani, G.; Barone, V.; Mennucci, B.; Petersson, G. A.; Nakatsuji, H.; Caricato, M.; Li, X.; Hratchian, H. P.; Izmaylov, A. F.; Bloino, J.; Zheng, G.; Sonnenberg, J. L.; Hada, M.; Ehara, M.; Toyota, K.; Fukuda, R.; Hasegawa, J.; Ishida, M.; Nakajima, T.; Honda, Y.; Kitao, O.; Nakai, H.; Vreven, T.; Montgomery, J. A., Jr.; Peralta, J. E.; Ogliaro, F.; Bearpark, M.; Heyd, J. J.; Brothers, E.; Kudin, K. N.; Staroverov, V. N.; Kobayashi, R.; Normand, J.; Raghavachari, K.; Rendell, A.; Burant, J. C.; Iyengar, S. S.; Tomasi, J.; Cossi, M.; Rega, N.; Millam, J. M.; Klene, M.; Knox, J. E.; Cross, J. B.; Bakken, V.; Adamo, C.; Jaramillo, J.; Gomperts, R.; Stratmann, R. E.; Yazyev, O.; Austin, A. J.; Cammi, R.; Pomelli, C.; Ochterski, J. W.; Martin, R. L.; Morokuma, K.; Zakrzewski, V. G.; Voth, G. A.; Salvador, P.; Dannenberg, J. J.; Dapprich, S.; Daniels, A. D.; Farkas, Ö.; Foresman, J. B.; Ortiz, J. V.; Cioslowski, J.; Fox, D. J. *Gaussian 09, Revision A.02*; Gaussian, Inc.: Wallingford, CT, 2010.
(32) Meena, J. S.; Thankachan, P. P. *Comput. Theor. Chem.* **2013**, *1024*, 1.
(33) Meena, J. S.; Thankachan, P. P. *J. Chem. Sci.* **2014**, *126*, 691.